Specialized SiO_2/TiO_2 Multilayered Coatings for Macroscopic Optical Force Sensors

Siyu Huang[1], Chunyang Gu[1], Tan Chen[1], and Fengzhou Fang[1,#]

1 State Key Laboratory of Precision Measuring Technology and Instruments, Laboratory of Micro/Nano Manufacturing Technology (MNMT), Tianjin University, Tianjin 300072, China
Corresponding Author / Email: fzfang@tju.edu.cn

KEYWORDS: Multilayered coatings, High-reflectivity, Optical force, Electrodynamics

Multilayered coatings are routinely used in optical devices to achieve their functions. In this study, a specialized multilayered coating is proposed which composed of alternating layers of SiO_2 and TiO_2 to create spectral gaps for varied incidents of high-power laser. The multilayered coating helps to achieve low-thermally induced fluctuations and effective optical force, which essentially ensures the performance of the optical force sensor. A theoretical framework for the analysis of the optical force in the multilayered coating is developed based on the Maxwell tensor of classical electrodynamics and the boundary conditions at the periodic interfaces. It is compatible with different numbers of layers. And the design, fabrication and measurement of the coating are demonstrated. The simulation and experiment results show that the multilayered coating can be employed to generate accurate optical force, which is consistent with the design. The study provides a new methodology for the control of optical forces and has a critical importance in the application of optical force on a macroscopic scale.

NOMENCLATURE

A_m = the absorption rate of the object's surface (1)
C_v = the specific heat capacity (J/(kg·K))
α = the linear elastic coefficient (Pa)
c_L = the longitudinal wave velocity (m/s)
c = the speed of light in a vacuum (m/s)
E = the electric field in time domain(V/m)
B = the magnetic flux density in time domain (T)
D = the electric displacement field in time domain (C/m^2)
H = the magnetic field in time domain (A/m)
M = the magnetization of material (A/m)
P = the polarization density of material (C/m^2)
ε_0 = the vacuum permittivity (F/m)
μ_0 = the vacuum permeability (H/m)
ρ_f = the free charge density (A/m^2)
$\mathbf{J}_f$ = the free current density (A/m^2)
f = the force density (N/m^3)
T = the stress tensor (Pa)
G = the momentum density (N·s/m^3)
ω = the very high optical frequency (s^{-1})
λ = the light wavelength (nm)
$\mathbf{E}_0$ = the electric field complex vector (V/m)
$\mathbf{H}_0$ = the magnetic field complex vector (A/m)
S = the Poynting Vector (W/m^2)
χ_E = the electric susceptibility (1)
χ_M = the magnetic susceptibility (1)
ϵ^{ijk} = the Levi-Civita tensor (1)

1. Introduction

The optical force effect is a phenomenon where a force is exerted on matter due to the exchange of momentum during the interaction between light and matter. This effect can provide precise and small forces ranging from piconewtons to millinewtons[1,2], which has led to significant and meaningful applications in the microscopic domain , such as in optical cooling and optical tweezers[3–6], where the size of the objects is less than the millimeter scale. In recent years, with the advancement of high-power laser technology, the study of the optical force effect has extended from the microscopic to the macroscopic scale, greatly expanding the research scope and potential applications. The optical force effect has advantages such as high sensitivity, rapid response, non-damaging, and traceability. It is expected to become a crucial breakthrough for the next generation of ultra-high precision optical sensing, measurement, and manufacturing technologies[7].

However, the phenomenon induced by the optical force on macroscopic objects, which primarily drives their motion, has extremely small magnitudes and susceptibility to be interfered with thermal effects. This makes the optical force difficult to be measured and applied through traditional techniques, necessitating the use of

specialized structures or devices with specialized coating[8–10].

Under a single laser pulse with an energy density of 1 J/cm², the motion driven by optical force on macroscopic elastic objects is only at the picometer scale, which exceeds the resolution of current sensors[11]. Additionally, thermal effects caused by laser absorption can induce thermoelastic effects, where the amplitude of thermoelastic motion is often much greater than that driven by optical force. Only when the absorption rate A_m of the object's surface is less than $2\kappa_m(1+\kappa_m)^{-1}$, the amplitude of thermoelastic motion will be smaller than that driven by optical force, where $\kappa_m = C_v/(\alpha c_L c)$. For optical glass substrates, a reflectivity of over 99.999% is required to meet the above conditions, which approaches the physical limit for reflective coatings, requiring the suppression of Brownian thermal motion in materials to achieve this[12].

Currently, ultra-high reflectivity coatings are primarily categorized into two types, metallic coatings and dielectric coatings. Metallic coatings, such as those made from gold or silver, have been widely used due to their high reflectivity in the visible and infrared regions. In 2017, a special gold coating reflector was used in the optical force measurement. This coating achieves an effective reflectivity over 99% in the experiment, which demonstrates the feasibility of metallic coatings for optical force research[13]. Dielectric coatings, typically composed of alternating layers of materials with different refractive indices, can achieve extremely low absorption and high reflectivity in designed waveband[12,14]. Dielectric coatings are most commonly used in the macroscopic optical force research. For example, Gu et al. designed and fabricated ultra-high reflectivity dielectric coatings, achieving a precise optical force of 132 nN with laser power of 20 W[15]. However, the specialized coatings as well as their theoretical framework for the optical force have not been reported so far. This study will fill the gap and address the unique challenges posed by optical force, showing importance to the macroscopic optical force research and applications.

2. Optical Force Calculation

The design and analysis of the specialized coating are based on the precise calculation of the optical fore. The maxwell stress tensor method is employed, and the time-averaging calculation makes it more practical.

2.1 Maxwell Stress Tensor Method

Maxwell's equations are the fundamental equations of electromagnetic theory, explaining the behavior of electromagnetic fields. Maxwell's equations consist of four equations: Gauss's law, which describes the generation of electric fields by charges; Gauss's law for magnetism, which asserts the nonexistence of magnetic monopoles; the Maxwell-Ampère law, which describes how electric currents and time-varying electric fields generate magnetic fields; and Faraday's law of induction, describing how time-varying magnetic fields generate electric fields, as shown in Eq.(1) to Eq.(4).

$$\nabla \cdot \mathbf{D} = \rho_{\mathrm{f}} \tag{1}$$

$$\nabla \cdot \mathbf{B} = 0 \tag{2}$$

$$\nabla \times \mathbf{E} = -\partial \mathbf{B}/\partial t \tag{3}$$

$$\nabla \times \mathbf{H} = \partial \mathbf{D}/\partial t + \mathbf{J}_{\mathrm{f}} \tag{4}$$

The equations discussed above are valid in any type of medium. The medium can influence the electromagnetic field through three effects: electric polarization, magnetization, and electrical conduction. The electromagnetic properties of a medium can be described by the following three constitutive relations: $\mathbf{H} = \mathbf{B}/\mu_0 - \mathbf{M}$, $\mathbf{D} = \mathbf{P} + \varepsilon_0\mathbf{E}$. In free space ($\mathbf{J}_{\mathrm{f}} = 0$, $\rho_{\mathrm{f}} = 0$), then $\mathbf{B} = \mu_0\mathbf{M}$, $\mathbf{D} = \varepsilon_0\mathbf{E}$, leading to the homogeneous Maxwell equation. The Maxwell stress tensor and momentum are represented as follows,

$$\mathbf{T} = (\varepsilon_0 E^2 + \mu_0 H^2)\bar{\bar{\mathbf{I}}}/2 - \varepsilon_0\mathbf{EE} - \mu_0\mathbf{HH} \tag{5}$$

$$\mathbf{G} = \mu_0\varepsilon_0\mathbf{E} \times \mathbf{H} \tag{6}$$

Based on the momentum continuity equation $\mathbf{f} = -\nabla \cdot \bar{\bar{\mathbf{T}}} - \partial\mathbf{G}/\partial t$ and the corresponding vector calculus laws, combined with Equations (1)-(4), the expression for the force density in the context of electrodynamics can be derived.

$$\mathbf{f} = \varepsilon_0(\nabla \cdot \mathbf{E})\mathbf{E} + \mu_0(\nabla \cdot \mathbf{H})\mathbf{H} + \mu_0\partial\mathbf{P}/\partial t \times \mathbf{H} + \mathbf{J}_{\mathrm{f}} \times \mu_0\mathbf{H} + \varepsilon_0\mathbf{E} \times \mu_0\partial\mathbf{M}/\partial t. \tag{7}$$

In Table 1, the subscripts M, A, e, eb, and eh represent the quantities in the electrodynamics formulations of Minkowski, Abraham, Einstein-Laub, Amperian, and Chu, respectively. For plane waves, and for a source-free environment, the expression for force density can be simplified into,

$$\mathbf{f} = \mu_0\partial\mathbf{P}/\partial t \times \mathbf{H} + \mathbf{J}_{\mathrm{f}} \times \mu_0\mathbf{H}. \tag{8}$$

Table 1 Different Formulations of Electrodynamics

$\mathbf{f}_{\mathrm{M}}$	$-\boldsymbol{E}^2\nabla\varepsilon/2-\boldsymbol{H}^2\nabla\mu/2+\rho\mathbf{E}+\mathbf{J}\times\mathbf{B}$
$\mathbf{T}_{\mathrm{M}}$	$(\mathbf{D}\cdot\mathbf{E} + \mathbf{B}\cdot\mathbf{H})/2-\mathbf{DE}-\mathbf{BH}$
$\mathbf{G}_{\mathrm{M}}$	$\mathbf{D}\times\mathbf{B}$
$\mathbf{f}_{\mathrm{A}}$	$-\boldsymbol{E}^2\nabla\varepsilon/2-\boldsymbol{H}^2\nabla\mu/2+\rho\mathbf{E}+\mathbf{J}\times\mathbf{B}+\partial(\mathbf{G}_{\mathrm{M}}-\mathbf{G}_{\mathrm{A}})/\partial t$
$\mathbf{T}_{\mathrm{A}}$	$(\mathbf{D}\cdot\mathbf{E} + \mathbf{B}\cdot\mathbf{H}-\mathbf{DE}-\mathbf{ED}-\mathbf{BH}-\mathbf{HB})/2$
$\mathbf{G}_{\mathrm{A}}$	$(\mathbf{E}\times\mathbf{H})/c^2$
$\mathbf{f}_{\mathrm{e}}$	$[\rho+(\mathbf{P}\cdot\nabla)]\mathbf{E}+(\mu_0\mathbf{M}\cdot\nabla)\mathbf{H}+(\mathbf{J}+\partial\mathbf{P}/\partial t)\times\mu_0\mathbf{H}-$
$\mathbf{T}_{\mathrm{e}}$	$(\varepsilon_0E^2+\mu_0H^2)\bar{\bar{\mathbf{I}}}/2-\mathbf{DE}-\mathbf{BH}$
$\mathbf{G}_{\mathrm{e}}$	$(\mathbf{E}\times\mathbf{H})/c^2$
$\mathbf{f}_{\mathrm{eb}}$	$-(\nabla\cdot\mathbf{P})\mathbf{E}+\partial\mathbf{P}/\partial t\times\mathbf{B}+(\nabla\times\mathbf{M})\times\mathbf{B}+\rho\mathbf{E}+\mathbf{J}\times\mathbf{B}$
$\mathbf{T}_{\mathrm{eb}}$	$(\varepsilon_0E^2+B^2/\mu_0)\bar{\bar{\mathbf{I}}}/2-\varepsilon_0\mathbf{EE}-\mathbf{BB}/\mu_0$
$\mathbf{G}_{\mathrm{eb}}$	$\varepsilon_0(\mathbf{E}\times\mathbf{B})$
$\mathbf{f}_{\mathrm{eh}}$	$[\rho-(\nabla\cdot\mathbf{P})]\mathbf{E}-(\nabla\cdot\mu_0\mathbf{M})\mathbf{H}+(\mathbf{J}+\partial\mathbf{P}/\partial t)\times\mu_0\mathbf{H}-$
$\mathbf{T}_{\mathrm{eh}}$	$(\varepsilon_0E^2+\mu_0H^2)\bar{\bar{\mathbf{I}}}/2-\varepsilon_0\mathbf{EE}-\mu_0\mathbf{HH}$
$\mathbf{G}_{\mathrm{eh}}$	$(\mathbf{E}\times\mathbf{H})/c^2$

Substituting the electromagnetic stress tensor and momentum density into the momentum continuity equation yields various optical force calculation formulas, as shown in Table 1. All the formulas in Table 1 can be used to calculate optical force, but the appropriate one should be selected based on the specific circumstances. Among them, $\mathbf{f}_{\mathrm{eh}}$ is particularly effective for calculating optical force at the interface between media, making it the most suitable for the continuous alternating characteristics of multilayered dielectric coatings.

2.2 The Time-Averaging Calculation

Due to the high optical frequency ω ($\omega = 2\pi c/\lambda$, on the order of 10^{15} s^{-1}), the instantaneous values of the optical force cannot be observed experimentally. Instead, only the average value over a time interval can be measured. It is assumed that the observation time is much longer than the photon oscillation period ($T = 2\pi/\omega$). Representing the electric and magnetic fields using complex vector

form,

$$\mathbf{E}(\boldsymbol{z},t)=\left[\boldsymbol{E}_0(z)e^{-i\omega t}+\boldsymbol{E}_0^*(z)e^{i\omega t}\right]/2, \quad (9)$$

$$\mathbf{H}(\boldsymbol{z},t)=\left[\boldsymbol{H}_0(z)e^{-i\omega t}+\boldsymbol{H}_0^*(z)e^{i\omega t}\right]/2, \quad (10)$$

where $\mathbf{E}_0(z)=\hat{\boldsymbol{x}}E_0e^{-ikz}$, $\mathbf{H}_0(z)=\hat{\boldsymbol{y}}H_0e^{-ikz}$, $\boldsymbol{E}=\boldsymbol{E}_0(z)e^{-i\omega t}$, $\boldsymbol{H}=\boldsymbol{H}_0(z)e^{-i\omega t}$. Then Eq. (8) can be rewritten in complex vector form,

$$\begin{aligned}\mathbf{f}=\rho(\boldsymbol{E}+\boldsymbol{E}^*)/2+\{&[(\boldsymbol{P}+\boldsymbol{P}^*)\cdot\nabla](\boldsymbol{E}+\boldsymbol{E}^*)\\&+[(\boldsymbol{M}+\boldsymbol{M}^*)\cdot\nabla](\boldsymbol{H}+\boldsymbol{H}^*)\\&+(\boldsymbol{J}+\boldsymbol{J}^*)\times\mu_0(\boldsymbol{H}+\boldsymbol{H}^*)\\&+\left(\dot{\boldsymbol{P}}+\dot{\boldsymbol{P}}^*\right)\times\mu_0(\boldsymbol{H}+\boldsymbol{H}^*)\\&-\mu_0\varepsilon_0\left(\dot{\boldsymbol{M}}+\dot{\boldsymbol{M}}^*\right)\times(\boldsymbol{E}+\boldsymbol{E}^*)\}/4. \quad (11)\end{aligned}$$

Substituting Eq. (9) and (10) into the Poynting Vector, which is defined as,

$$\mathbf{S}=\mathbf{E}\times\mathbf{H}. \quad (12)$$

By applying the distributive property of vector operations, we obtain an expression consisting of four terms, two of which include factor $e^{2i\omega t}$ and $e^{-2i\omega t}$ respectively. Averaging these two terms over the observation interval t $(-T'\ll t\ll T',\ T'\gg T)$,

$$(2T')^{-1}\int_{-T'}^{T'}e^{-2i\omega t}\mathrm{d}t=(T/T')\sin(2\omega T')/4\pi. \quad (13)$$

Due to $T/T'\ll 1$, the integrals containing $e^{-2i\omega t}$ and $e^{2i\omega t}$could be neglected. Thus, the time-averaged value of the Poynting vector is given by,

$$\langle\mathbf{S}\rangle=\frac{1}{2T'}\int_{-T'}^{T'}\mathbf{S}\mathrm{d}t=\frac{1}{2}\mathrm{Re}(\mathbf{E}_0\times\mathbf{H}_0^*). \quad (14)$$

Therefore, the time-dependent terms in Eq. (11) can be neglected, then, using the Cartesian tensor operations, we further derive Eq. (11)

$$\begin{aligned}\langle\mathbf{f}\rangle=\mathrm{Re}[&\varepsilon_0\chi_E E_i\partial^i E_j^*+\chi_m H_i\partial^i H_j^*+\mu_0\varepsilon_0\omega_0\epsilon^{ijk}(\chi_E\\&-\chi_m)E_jH_k^*]/2, \quad (15)\end{aligned}$$

Substituting it into the Eq. (7),

$$\langle\mathbf{f}\rangle_x=\hat{\boldsymbol{x}}\mu_0\varepsilon_0\omega_0\mathrm{Im}[(\chi_E-\chi_m)\mathbf{E}\times\mathbf{H}^*]/2, \quad (16)$$

which represents the time-averaged expression of the optical force along the propagation direction, indicating the magnitude of optical force exerted on a unit volume of the medium. Here, $\chi_E=\mathbf{P}/\varepsilon_0\mathbf{E}$ and $\chi_M=\mathbf{M}/\mathbf{H}$. For Minkowski and Abraham formulation, the time-averaging expression can be written as,

$$\langle\mathbf{f}\rangle_{y,z}=-\hat{\boldsymbol{z}}\nabla\varepsilon\mathrm{Re}[\mathbf{E}\cdot\mathbf{E}^*]/4-\hat{\boldsymbol{y}}\nabla\mu\mathrm{Re}[\mathbf{H}\cdot\mathbf{H}^*]/4, \quad (17)$$

where the gradient operator needs to be applied to the material parameters ε and μ. This equation yields values only at point where material is discontinuous. Consequently, the computed values from further calculation cannot represent the true values, but rather indicate the presence of a discontinuous force at these interfaces.

3. Results and Discussion

Based on the calculation, a specialized coating was designed and fabricated for the optical force device. The optical force exerting on the designed multilayered dielectric coating is discussed when irradiated by a plane wave in an ambient air environment. A two-dimensional plane wave irradiation model of the coating is established using the finite element method. Considering the differences between actual experimental parameters and simulation parameters, as well as computational limitations, the numerical calculation model of the electromagnetic field is proportionally scaled down. The diameter of the actual optical force sensor with the coating is 20 mm, and the laser beam radius is 5 mm. In the finite element simulation, the region is scaled down to a diameter of 10 μm, and the beam diameter is reduced to 2.5 μm.

The specialized multilayered coating is composed of alternating layers of SiO_2 and TiO_2 to achieve high reflectivity both at 1064 nm and 632.8 nm. The 1064 nm corresponds to the excitation high power laser, and the 632.8 nm corresponds to the measurement laser. The substrate material is optical glass. The picture and measurement of the coating are shown in the Fig. 1.

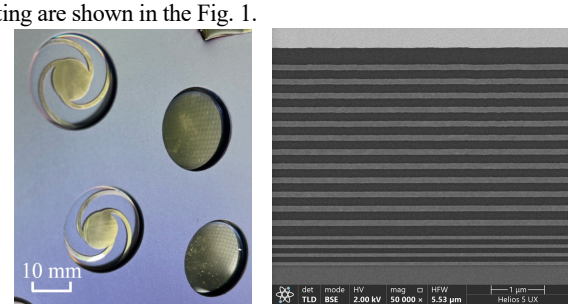

Fig. 1 The SiO_2 / TiO_2 multilayered coated optical sensors (left: SiO_2/TiO_2 multilayered coating; right: Scanning electron microscope measurement of the multilayered coating)

The coating is fabricated by the ion-assisted evaporation method. The coating has a multilayer Bragg reflective structure, with SiO_2 and TiO_2 as the materials. The refractive indices of these materials at a wavelength of 1064 nm are 1.4496 and 2.47958. The SiO_2 and TiO_2 layers are alternately deposited. The first layer is SiO_2 at a thickness of 366.99 nm, the second layer TiO_2 is 107.30 nm, and the third layer SiO_2 is 183.49 nm. Subsequent layers are alternately deposited using the materials and thicknesses of the second and third layers, resulting in a total coating thickness of 4460.88 nm. After the coating process, the device needs to be left in a dry cabinet for 48 hours to release residual stress from the coating. The measured reflectivity of the coating is 99.99% at 1064 nm and 86.07% at 632.8 nm.

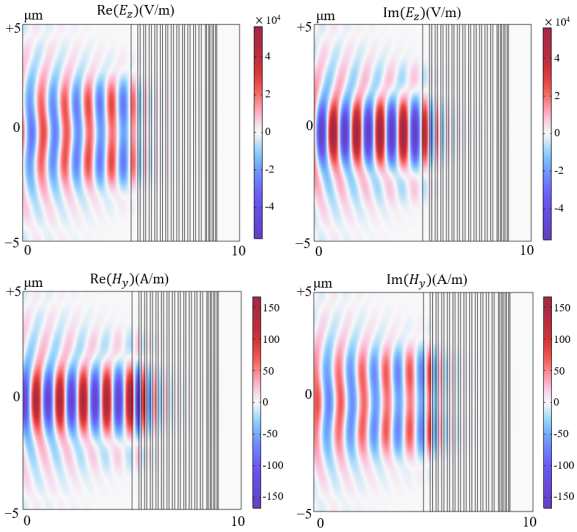

Fig. 2 Two-dimensional electric field and magnetic field distribution within and around the multilayered coatings.

By applying the calculation formula of optical force discussed in Section 2, the distribution of the optical force over the two-dimensional simulation region is numerically computed, with results shown in Fig.2 and Fig. 3. The direction of the red arrow represents the direction of the optical force. It indicates that the beam propagating along the z-axis

exerts force along the propagation direction on the coating. The simulation results show that the peak optical force is 1.28×10^{5} N/m^3. Integrating the peak optical force over the two-dimensional surface area and dividing by the beam width yields the average optical force within the irradiated region of 7.39×10^{-3} N/m^3 .Compared to the designed value, the final value is consistent, which is verified in the experiment[15].

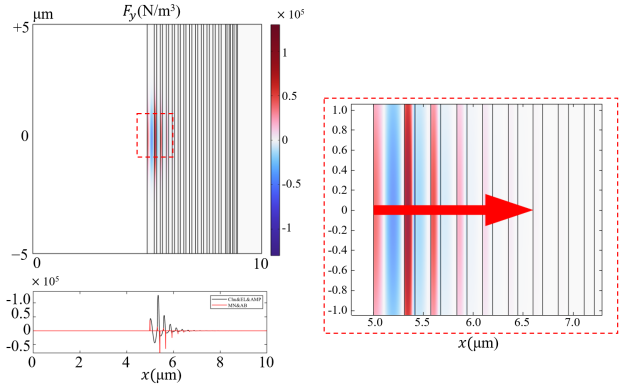

Fig. 3 Distribution of the optical force within the SiO_2 / TiO_2 multilayered coating

Simulations on the optical force at the coating interfaces is also conducted by combining the Minkowski and Abraham formulations, as shown in Fig. 3. The two first terms in $\mathbf{f}_M$ and $\mathbf{f}_A$ in Table 1 give the density of force acting on the regions of spatial inhomogeneity. This demonstrates the good compatibility of the coating.

4. Conclusion

This study provides a detailed derivation and analysis of the optical force calculation models for a specialized coatings using the Maxwell stress tensor. Based on the finite element method, an electromagnetic field model for multilayered coating is established, and the optical force exerted on the coating is accurately calculated. Based on the simulation and experiment results, the specialized coating can be employed to meet the following four requirements:

- The designed optical force over 100 nN is foremost achieved in devices with a centimeter scale and milligram-level mass.
- The high reflectivity over 99.9% is achieved to suppress thermal effects.
- The distribution of the optical force facilitates the macroscopic device research which can be treated as surface force.
- Non-contact ultra-precise laser interferometry measurement is guaranteed by dual-band high reflection.

These four requirements can be also treated as coating standards in the related macroscopic optical force research and applications. They essentially ensure the performance of the macroscopic optical force device.

ACKNOWLEDGEMENT

This study was supported financially by the National Natural Science Foundation (Np. 52035009). Thanks extend to Zhongdu He, Jinyan Lv for the support to the experiments.

REFERENCES

1. Jia, Q., Lyu, W., Yan, W., Tang, W., et al. "Optical Manipulation: From Fluid to Solid Domains," Photonics Insights, Vol. 2, pp. R05, 2023.
2. Mansuripur, M. "Radiation Pressure and the Linear Momentum of the Electromagnetic Field," Opt. Express, Vol. 12, No. 22, pp. 5375–5401, 2004.
3. Gieseler, J., Deutsch, B., Quidant, R., Novotny, L. "Subkelvin Parametric Feedback Cooling of a Laser-Trapped Nanoparticle," Phys. Rev. Lett., Vol. 109, No. 10, pp. 103603, 2012.
4. Barker, P. F., Shneider, M. N. "Cavity Cooling of an Optically Trapped Nanoparticle," Phys. Rev. A, Vol. 81, No. 2, pp. 023826, 2010.
5. Kolbow, J. D., Lindquist, N. C., Ertsgaard, C. T., Yoo, D., et al. "Nano-optical Tweezers: Methods and Applications for Trapping Single Molecules and Nanoparticles," ChemPhysChem, Vol. 22, No. 14, pp. 1409–1420, 2021.
6. Polimeno, P., Magazzu, A., Iati, M. A., Patti, F., et al. "Optical Tweezers and Their Applications," J. Quant. Spectrosc. Radiat. Transf., Vol. 218, pp. 131–150, 2018.
7. Fang, F. "On the Three Paradigms of Manufacturing Advancement," Nanomanuf. Metrol., Vol. 6, No. 1, pp. 35, 2023.
8. Bonifacio, L. D., Lotsch, B. V., Puzzo, D. P., Scotognella, F., et al. "Stacking the Nanochemistry Deck: Structural and Compositional Diversity in One-Dimensional Photonic Crystals," Adv. Mater., Vol. 21, No. 16, pp. 1641–1646, 2009.
9. Cole, G. D., Zhang, W., Bjork, B. J., Follman, D., et al. "High-Performance near- and Mid-Infrared Crystalline Coatings," Optica, Vol. 3, No. 6, pp. 647, 2016.
10. Kolodziej, T., Shvyd'ko, Y., Shu, D., Kearney, S., et al. "High Bragg Reflectivity of Diamond Crystals Exposed to Multi-kW Mm-2 X-Ray Beams," J. Synchrotron Radiat., Vol. 25, No. Pt 4, pp. 1022–1029, 2018.
11. Fleming, A. J. "A Review of Nanometer Resolution Position Sensors: Operation and Performance," Sens. Actuators Phys., Vol. 190, pp. 106–126, 2013.
12. Cole, G. D., Zhang, W., Martin, M. J., Ye, J., et al. "Tenfold Reduction of Brownian Noise in High-Reflectivity Optical Coatings," Nat. Photonics, Vol. 7, No. 8, pp. 644–650, 2013.
13. Yuan, Y., Gu, C., Cao, Y., Wang, S., et al. "Observation of Radiation Pressure Induced Deformation of High-Reflective Reflector," J. Phys. Commun., Vol. 1, No. 5, pp. 055031, 2017.
14. Požar, T., Laloš, J., Babnik, A., Petkovšek, R., et al. "Isolated Detection of Elastic Waves Driven by the Momentum of Light," Nat. Commun., Vol. 9, No. 1, pp. 3340, 2018.
15. Gu, C., Huang, S., Fang, F. "Optimized Design and Experimental Study of a Macroscopic Mirror to Achieve Linear Amplification of Optical Force-Induced Displacement," Opt. Express, Vol. 31, No. 18, pp. 28830, 2023